NOTICE CONCERNING COPYRIGHT RESTRICTIONS

Inferring In-Situ and Immobile Water Saturations from Field Measurements

Rodolfo P. Belen Jr. and Roland N. Horne

Stanford Geothermal Program, Stanford University, Stanford, CA 94305-2220, USA
http://ekofisk.stanford.edu/geotherm.html

ABSTRACT

This study developed models of vapor and liquid geothermal reservoirs, based on Darcy's law and material and energy conservation equations. These models can be used as tools to infer the in-situ and immobile water saturations from field measurements of cumulative mass production, discharge enthalpy and temperature. The knowledge of the in-situ and immobile water saturations is valuable in evaluating geothermal reservoir performance.

Knowing rock and fluid properties, and the difference between the stable initial, T_o, and dry-out, T_d, downhole temperatures, the in-situ and immobile water saturations of vapor-dominated reservoirs can be estimated. On the other hand, the in-situ and immobile water saturation, and the change in mobile water content of liquid-dominated reservoirs can be inferred from the cumulative mass production, Δm, and enthalpy, h', data.

Comparison with two-phase radial flow simulation results confirmed the validity and usefulness of these models.

Introduction

The discharge of saturated or superheated steam during the exploitation of vapor-dominated geothermal reservoirs greatly exceeds what can be stored as vapor. Therefore, vapor-dominated reservoirs must contain substantial amounts of liquid water to sustain production (James, 1968; Nathenson 1975; Grant, 1979). In describing the response of vapor-dominated reservoirs to exploitation, it is valid to assume that the liquid water is completely immobile. Although water may be slightly mobile in the natural state of the reservoir, it is soon immobile because the water saturation drops as fluids are produced (Grant, 1979). The liquid water is adsorbed in the pores of the reservoir matrix and is able to vaporize, but is not able to flow as liquid water.

Grant (1979) estimated the in-place water saturation of the Kawah Kamojang geothermal field, Java, based on variations in the gas content of the production fluids. Changing the flow rate at the wellhead produces a response in the reservoir pressure and gas content, which allows for the estimation of the in-place water saturation. In contrast, this study aims to infer the in-situ and immobile water saturations from field measurements of changes in the flowing enthalpies of producing wells as well as downhole wellbore temperatures.

Zero-dimensional models can be used to describe the pressure, temperature and saturation profiles accompanying production. This study developed models of both vapor and liquid dominated geothermal reservoirs that can be used to infer the in-situ and immobile water saturation from field measurements of cumulative mass production, enthalpy and temperature.

Zero-Dimensional Models

Darcy's law and the differential material and energy conservation equations that describe the response of geothermal reservoirs to exploitation can be combined to form simple zero-dimensional models. For the case of vapor dominated geothermal systems, the only mobile phase is steam. The flow of dry steam can be described by Equations 1 to 3. It is assumed that the immobile water does not impede the flow of steam and that the steam flow is governed by Darcy's law.

$$\phi\frac{\partial}{\partial t}\{s\rho_w+(1-s)\rho_s\}=-\nabla\cdot(\vec{u}_s\rho_s) \qquad (1)$$

$$\frac{\partial}{\partial t}\{(1-\phi)\rho_r c_r T+\phi s\rho_w h_w+\phi(1-s)\rho_s h_s\}=-\nabla\cdot(\vec{u}_s\rho_s h_s) \qquad (2)$$

$$\vec{u}_s=-\frac{kk_{rs}}{\mu_s}\nabla p \qquad (3)$$

Under reservoir conditions, the enthalpy of saturated steam is nearly constant with temperature. This approximation results in a simplified relation between pressure and saturation at any point in the reservoir.

$$(1-\phi)\rho_r C_r T+\phi s\rho_w(h_w-h_s)=\text{constant} \qquad (4)$$

Reduction in the reservoir pressure resulting from production is accompanied by a reduction in reservoir temperature to main-

tain saturation conditions. Heat must then be mined from the rock to cool it, which is achieved by vaporizing some of the liquid water to steam. Therefore, a decline in the reservoir pressure results in a decline in the reservoir liquid saturation. This mining of heat and consequent decline in liquid saturation continues as long as saturation conditions exist. The saturation falls to zero at dry out conditions and the in-place water saturation can then be estimated using the initial and dry out reservoir conditions (Grant 1979).

$$s_o = \frac{(1-\phi)}{\phi}\frac{\rho_r c_r (T_o - T_d)}{\rho_w (h_s - h_w)_{T_o}} \tag{5}$$

This zero-dimensional model allows the calculation of the in-situ water saturation using rock and fluid properties and the initial, T_o, and dry-out, T_d, downhole or reservoir temperatures. In this case, the dry-out temperature is that temperature at which the reservoir has completely dried out and has started to produce superheated steam.

On the other hand, for the liquid dominated reservoir case, the differential material and energy balance equations (Equations 6 and 7) and the simplified equations describing the zero-dimensional model (Equations 8 and 9) are much more complicated because both water and steam phases are mobile.

$$\phi \frac{\partial}{\partial t}\{s\rho_w + (1-s)\rho_s\} = -\nabla \cdot (\vec{u}_w \rho_w + \vec{u}_s \rho_s) \tag{6}$$

$$\frac{\partial}{\partial t}\{(1-\phi)\rho_r c_r T + \phi s \rho_w h_w + \phi(1-s)\rho_s h_s\} = -\nabla \cdot (\vec{u}_w \rho_w h_w + \vec{u}_s \rho_s h_s) \tag{7}$$

$$\phi V \Delta(s\rho_w) + \phi V \Delta\{(1-s)\rho_s\} + m_w' + m_s' = 0 \tag{8}$$

$$\phi V \Delta(s\rho_w h_w) + \phi V \Delta\{(1-s)\rho_s h_s\} + (1-\phi) V \rho_r C_r \Delta T + m_w' h_w' + m_s' h_s' = 0 \tag{9}$$

The composition and enthalpy of the production fluids is determined by the mobility of steam and liquid water in the porous rock given by the relative permeabilities and viscosities of the two phases as shown in Equations 10 and 11.

$$m_w' = \frac{\rho_w \dfrac{k_{rw}}{\mu_w}}{\rho_w \dfrac{k_{rw}}{\mu_w} + \rho_s \dfrac{k_{rs}}{\mu_s}} \Delta m \tag{10}$$

$$m_s' = \frac{\rho_s \dfrac{k_{rs}}{\mu_s}}{\rho_w \dfrac{k_{rw}}{\mu_w} + \rho_s \dfrac{k_{rs}}{\mu_s}} \Delta m \tag{11}$$

Simulated Two-Phase Radial Flow Model

The zero-dimensional models shown in the previous section assume that the pressures, temperatures and saturations are uniform throughout the reservoir. These models do not take into account the transient and spatial effects of two-phase flow in the reservoir. In order to investigate the validity and usefulness of these models in determining the in-situ and immobile saturations, two-phase radial flow was modeled using the reservoir simulator TOUGH2. The TOUGH2 simulation results were then compared with those predicted by the zero-dimensional models.

A cylindrical reservoir model was used in the TOUGH2 simulation runs. Reservoir radius is 1 kilometer and thickness is 10 meters. The model consists of 100 grid blocks and the grid size increases logarithmically from the center to the boundary of the reservoir. Initial reservoir temperature is 280°C. A single production well maintained at constant downhole wellbore pressure of 200 psia is located in the middle of the reservoir. Reservoir rock properties used in the simulation are those of Geysers geothermal rocks, which are tabulated below.

Table 1. Geysers geothermal rock properties.

Porosity	5%
Permeability	1 x 10^{-13} m^2
Rock density	2600 kg/m^3
Rock specific heat	485 J/kg(C

Figures 1 to 3 are semilog plots of the saturation, temperature and pressure profiles with time and radial distance from the well. Initially, water saturation throughout the reservoir in this particular simulation run is 0.3. As a response to production, reservoir pressure, temperature and saturation drop and boiling near the wellbore commences. The boiling front moves farther into the reservoir away from the well as two-phase steam is produced. However, water saturation stays above and never goes below the immobile water saturation. The reservoir eventually produces dry saturated steam. During this time, reservoir saturation has dropped below the immobile water saturation. Water remaining in the reservoir during this period is immobile water, which is able to vaporize but not able to flow.

At some point during production, the reservoir completely dries out and starts to produce superheated steam. Water saturation has dropped to zero throughout the reservoir. The sequence of events in the production history of the reservoir is labeled in Figure 1.

Comparison of Two-Phase Radial Flow Model with Zero-Dimensional Model

Figure 4 compares the production enthalpies and reservoir temperatures simulated by TOUGH2 with those predicted by the zero-dimensional model for a vapor-dominated reservoir case with in-situ water saturation equal to 0.3. There appears to be a very good agreement between the simulation and the modeling

results. TOUGH2 simulation results were then used to calculate the in-situ water saturation using Equation 5 as shown in the following calculation.

$$s_o = \frac{(1-\phi)}{\phi}\frac{\rho_r c_r (T_o - T_d)}{\rho_w (h_s - h_w)_{T_o}} = \frac{(1-0.05)}{0.05}\frac{(2600\,kg/m^3)(0.485\,kJ/kg°C)(280.0°C - 266.5°C)}{750.5\,kg/m^3\,(2780.4\,kJ/kg - 1236.8\,kJ/kg)} = 0.30$$

The zero-dimensional model gave the correct in-situ water saturation, which in this case is equal to the immobile water saturation. This result confirms that the zero-dimensional model can be used to infer both the in-place and immobile water saturation of vapor dominated geothermal reservoirs by knowing the initial and dry-out reservoir temperatures.

The TOUGH2 simulated reservoir temperatures agreed satisfactorily with the modeled temperatures. However, reservoir temperatures are not normally measured in the field. Instead, surface and downhole temperatures are routinely measured in the production wells. Figure 5 is a plot comparing TOUGH2 simulated downhole temperatures and modeled reservoir temperatures. The sudden initial drop in the downhole wellbore temperature as a response to production is clearly evident from the plot. After this early transient period, downhole temperatures decline at the same rate as the reservoir temperatures. TOUGH2 simulated downhole temperatures were then used to estimate the in-situ water saturation using Equation 5. The initial temperature, T_o, was taken to be the stable temperature after the early transient period. The zero-dimensional model still gave a very close approximation of the correct in-situ water saturation as shown in the following calculation.

$$s_o = \frac{(1-\phi)}{\phi}\frac{\rho_r c_r (T_o - T_d)}{\rho_w (h_s - h_w)_{T_o}} = \frac{(1-0.05)}{0.05}\frac{(2600\,kg/m^3)(0.485\,kJ/kg°C)(251.5°C - 238.0°C)}{750.5\,kg/m^3\,(2780.4\,kJ/kg - 1236.8\,kJ/kg)} = 0.28$$

Therefore, either downhole wellbore or reservoir temperatures can be used to estimate the in-place water saturation using the zero-dimensional model. However, it is important that the stable initial, T_o, and dry-out, T_d, downhole temperatures be used in Equation 5.

$$s_o = \frac{(1-\phi)}{\phi}\frac{\rho_r c_r (T_o - T_d)}{\rho_w (h_s - h_w)_{T_o}} \qquad (5)$$

On the other hand, the response of liquid dominated geothermal reservoirs to exploitation can be described by a sequence of two-phase, dry saturated and superheated steam production. TOUGH2 and the zero-dimensional model predict similar trends in production enthalpy and temperature as illustrated in Figures 6 to 8. The enthalpy of produced two-phase steam increases and reservoir temperature declines as the reservoir gets depleted of its mobile water. The production enthalpy then plateaus as the reservoir continues to dry out and produces dry saturated steam while the temperature continues to fall almost linearly. Finally, the enthalpy increases further as the reservoir completely dries out of immobile water and produces superheated steam.

However, the zero-dimensional model, which does not take into account both transient and spatial variations in temperature, pressure and saturation, fails to match the early transient two-phase production period predicted by TOUGH2. The zero-dimensional model predicts a continuous increase in two-phase steam enthalpy with cumulative mass production. On the other hand, TOUGH2 predicts a production period of apparently stable two-phase steam enthalpy immediately after the early transient period. Then the enthalpy increases with production until dry saturated steam is produced.

Interesting observations can be made from the modeling results. Figures 9 and 10 are plots of production enthalpy and temperature for different values of in-situ water saturation and a fixed immobile water saturation. On the other hand, Figures 11and 12 are plots for different values of immobile water saturation and a fixed in-situ water saturation.

Based on the modeling results, two-phase steam enthalpies are a function of the mobile water content of the reservoir, that is, the difference between the initial and immobile water saturation. Reservoirs with higher mobile water saturations produce two-phase steam with lower enthalpies. This is clearly evident from Figures 13 and 14, which show production enthalpies for cases of constant mobile water content but varying in-situ and immobile water saturation. Likewise, dry-out temperatures follow the same trend. Reservoirs with higher mobile water content dry-out at lower temperatures. Furthermore, dry saturated steam production commences at a later time in the life of a reservoir containing greater amount of mobile water.

The mobile water content and the immobile water saturation of liquid-dominated geothermal reservoirs can then be inferred from the two-phase steam production enthalpy and the cumulative mass production using the zero-dimensional model. The discharge enthalpy of two-phase steam can be expressed as a weighted average of the individual steam and liquid water enthalpies given by Equation 12.

$$h' = \frac{\rho_w \frac{k_{rw}}{\mu_w} h_w + \rho_s \frac{k_{rs}}{\mu_s} h_s}{\rho_w \frac{k_{rw}}{\mu_w} + \rho_s \frac{k_{rs}}{\mu_s}} \qquad (12)$$

Assuming that linear steam-liquid water relative permeability relations are valid, the above equation can be rearranged to obtain an expression for the mobile water content in the reservoir,

$$\frac{s - s_{wr}}{1 - s_{wr} - s_{sr}} = \frac{\frac{\rho_s}{\mu_s}(h_s - h')}{\frac{\rho_w}{\mu_w}(h' - h_w) + \frac{\rho_s}{\mu_s}(h_s - h')} \qquad (13)$$

Equation 13 can be used to calculate the ratio of the mobile water in the reservoir to the maximum possible mobile water. This ratio gives an indication of how much mobile water is present in the reservoir and how fast the reservoir is drying out. Similar expressions can be obtained by assuming different relative permeability relations.

The change in the reservoir saturation from an initial to a final state can be estimated using cumulative mass production data. The material balance equation describing two-phase steam production can be simplified to Equation 14 by assuming that

the densities of steam and liquid water are approximately invariant with pressure and temperature. This equation gives the change in reservoir saturation as a function of the cumulative mass production, (Δ, knowing the reservoir pore volume, ϕV.

$$\Delta s = s_1 - s_2 = \frac{\Delta m}{\phi V(\rho_w - \rho_s)} \tag{14}$$

The immobile water saturation can then be estimated based on the change in mobile water content from Equation 13 and the change in reservoir saturation from Equation 14. This technique is demonstrated below using fluid properties, and enthalpy and cumulative mass production values simulated by TOUGH2. It is important to note that in using the model, the densities and viscosities of the two phases as well as the enthalpy of saturated steam are assumed to be invariant with pressure and temperature.

T°C	h' kJ/kg	ρ_w kg/m³	ρ_s kg/m³	μ_w cp	μ_s cp	h_w kJ/kg	h_s kJ/kg
280	2144	750.5	33.2	0.55	0.11	1237	2780
274	2645	750.5	33.2	0.55	0.11	1070	2780

Calculate the mobile water content at the initial state using Equation 13.

$$\frac{s_1 - s_{wr}}{1 - s_{wr} - s_{sr}} = \frac{\frac{\rho_s}{\mu_s}(h_s - h')}{\frac{\rho_w}{\mu_w}(h' - h_w) + \frac{\rho_s}{\mu_s}(h_s - h')} = 0.1334$$

Calculate the mobile water content at the final state using Equation 13.

$$\frac{s_2 - s_{wr}}{1 - s_{wr} - s_{sr}} = 0.0185$$

Calculate the difference in mobile water between the initial and final states.

$$\frac{\Delta s}{1 - s_{wr} - s_{sr}} = \frac{s_1 - s_{wr}}{1 - s_{wr} - s_{sr}} - \frac{s_2 - s_{wr}}{1 - s_{wr} - s_{sr}} = \frac{s_1 - s_2}{1 - s_{wr} - s_{sr}} = 0.1149$$

Calculate the change in reservoir saturation using Equation 14.

$$\Delta s = s_1 - s_2 = \frac{\Delta m}{\phi V(\rho_w - \rho_s)} = \frac{8.13 \times 10^7 kg}{0.05(\pi \cdot 1000^2 \cdot 10m^3)(750.5 kg/m^3 - 33.2 kg/m^3)} = 0.0722$$

Calculate the immobile water saturation based on the change in mobile water content and the change in reservoir saturation.

$$1 - s_{wr} - s_{sr} = \frac{\Delta s}{\frac{\Delta s}{1 - s_{wr} - s_{sr}}} = \frac{0.0722}{0.1149} = 0.63$$

$$s_{sr} = 0.1, \quad \textit{therefore,} \quad s_{wr} = 0.27 \approx 0.3$$

Conclusions and Recommendations

The in-situ and immobile water saturations can be inferred from field measurements of cumulative mass production, enthalpy and downhole temperature using simple zero-dimensional models developed based on material and energy conservation equations and Darcy's law. For vapor-dominated reservoirs, the in-situ and immobile water saturation can be estimated knowing rock and fluid properties, and the difference between the stable initial and the dry-out downhole temperatures and using Equation 5.

$$s_o = \frac{(1-\phi)}{\phi} \frac{\rho_r c_r (T_o - T_d)}{\rho_w (h_s - h_w)_{T_o}} \tag{5}$$

On the other hand, the in-situ and immobile water saturation of liquid dominated reservoirs can be inferred from cumulative mass production, enthalpy, and downhole temperature data using Equations 13 and 14.

$$\frac{s - s_{wr}}{1 - s_{wr} - s_{sr}} = \frac{\frac{\rho_s}{\mu_s}(h_s - h')}{\frac{\rho_w}{\mu_w}(h' - h_w) + \frac{\rho_s}{\mu_s}(h_s - h')} \tag{13}$$

$$\Delta s = s_1 - s_2 = \frac{\Delta m}{\phi V(\rho_w - \rho_s)} \tag{14}$$

The validity and usefulness of these zero-dimensional models were verified by comparing the modeling results with TOUGH2 two-phase radial flow simulation results. It is recommended that actual field production data be used to further verify the validity and usefulness of these models.

Acknowledgement

This research was conducted with financial support through the Stanford Geothermal Program under the US Department of Energy Grant No. DE-FG07-95ID13370.

References

Atkinson P., Celati R., Corsi R., Kucuk F., and Ramey Jr. H.: "Thermodynamic behavior of the Bagnore geothermal field", *Geothermics*, Volume 7, (1977), 185-208.

Grant M.: "Water Content of the Kawah Kamojang Geothermal Reservoir", *Geothermics*, Volume 8, (1979), 21-30.

Grant M.: "Broadlands – a gas dominated geothermal field", *Geothermics*, Volume 6, (1977), 9-29.

Horne R.: Notes on Geothermal Reservoir Engineering, Stanford University, Stanford, California (1991).

Moench, A and Atkinson, P.: "Transient-Pressure Analysis in Geothermal Steam Reservoirs with an Immobile Vaporizing Liquid Phase", *Geothermics*, Volume 7, (1978), 253-264.

Nathenson, M.: "Some Reservoir Engineering Calculations for the Vapor Dominated System at Larderello, Italy", U.S. Geological Survey Open-file Report 75-142, April 1975.

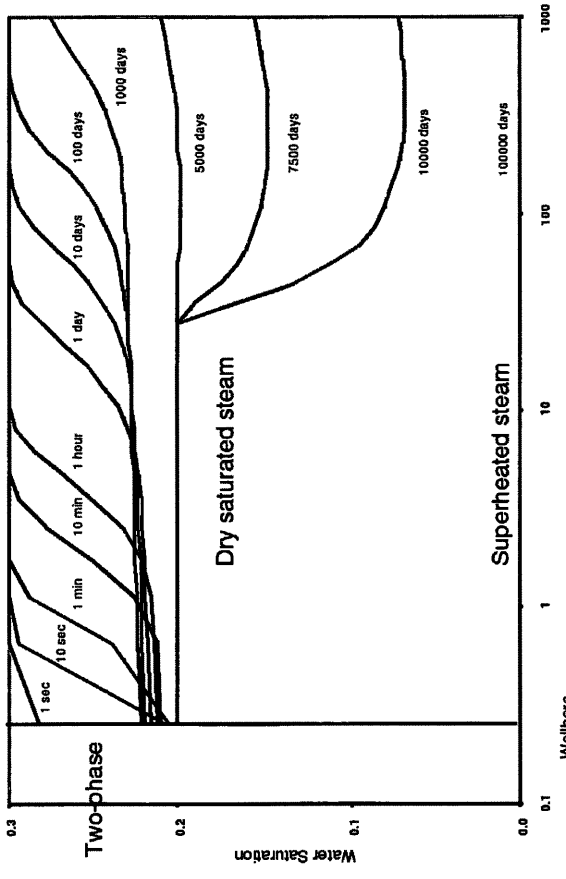

Figure 1. Water saturation profile with distance and time: $s_{wi} = 0.3$; $s_{wr} = 0.2$.

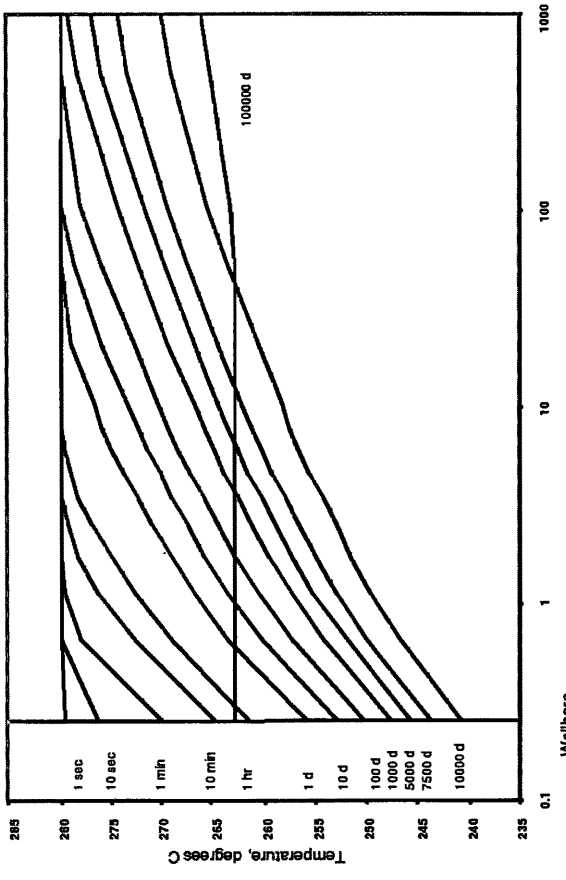

Figure 2. Temperature profile with distance and time: $s_{wi} = 0.3$; $s_{wr} = 0.2$.

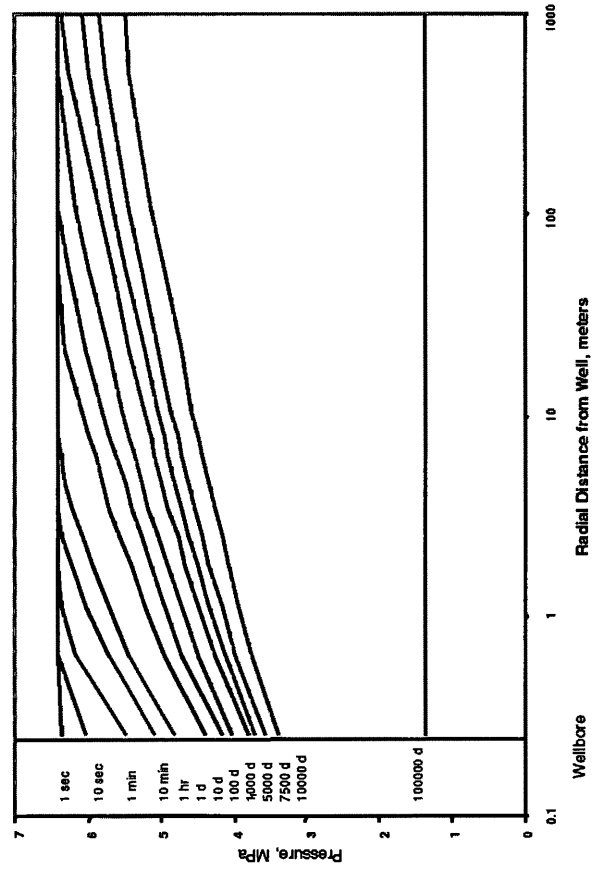

Figure 3. Pressure profile with distance and time: $s_{wi} = 0.3$; $s_{wr} = 0.2$.

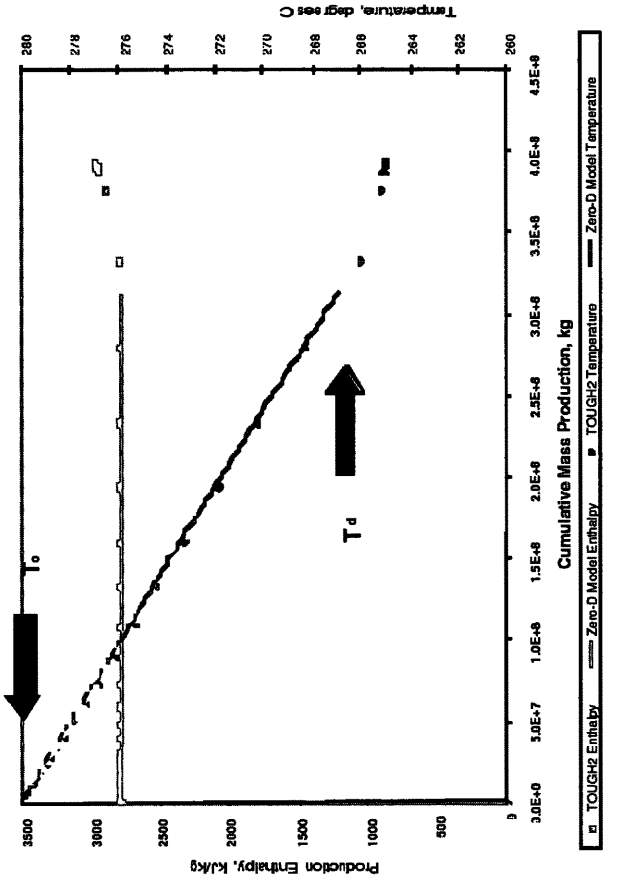

Figure 4. Production enthalpy and reservoir temperature profiles: $s_{wi} = 0.3$; $s_{wr} = 0.3$.

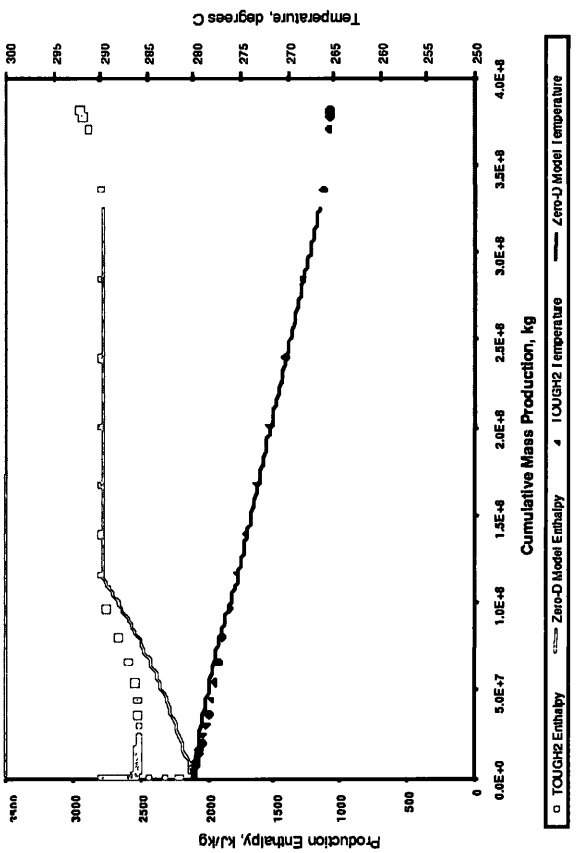

Figure 6. Production enthalpy and production temperature profiles: $s_{wi} = 0.3$; $s_{wr} = 0.2$

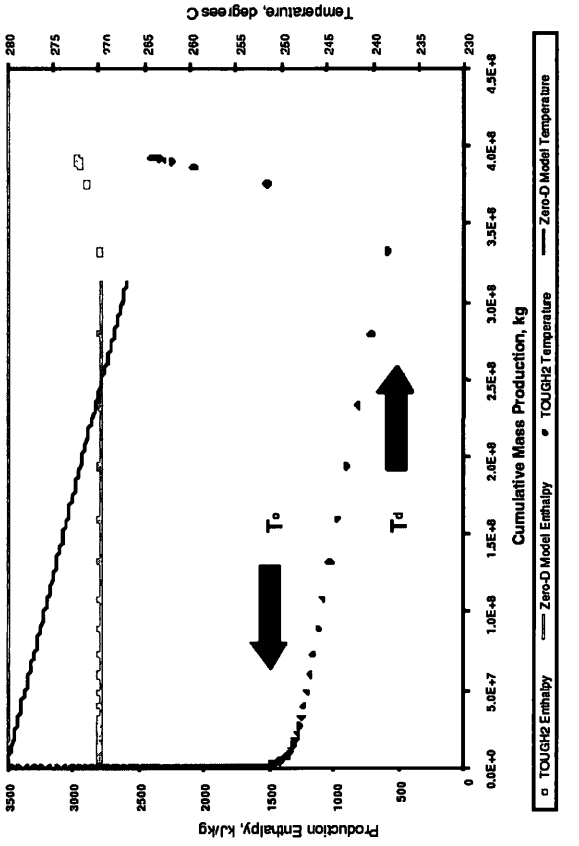

Figure 5. Production enthalpy and production temperature profiles: $s_{wi} = 0.3$; $s_{wr} = 0.3$.

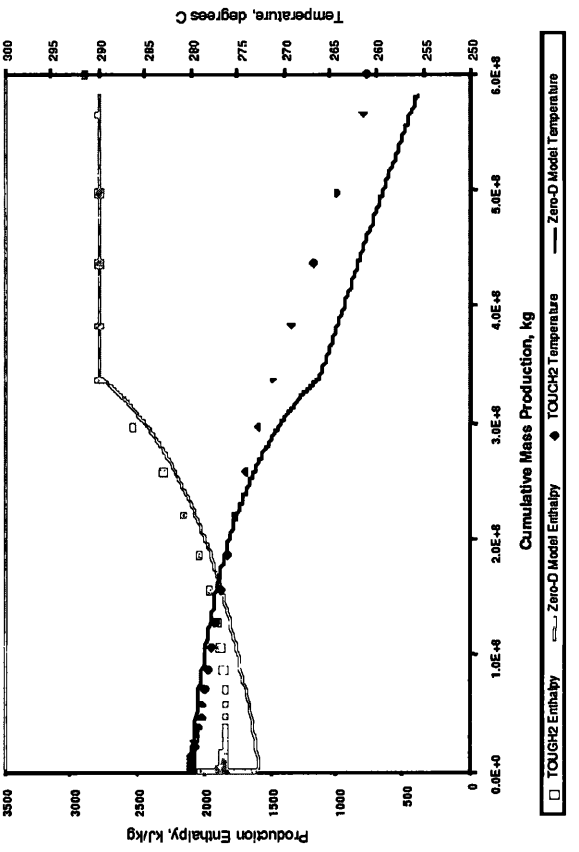

Figure 8. Production enthalpy and production

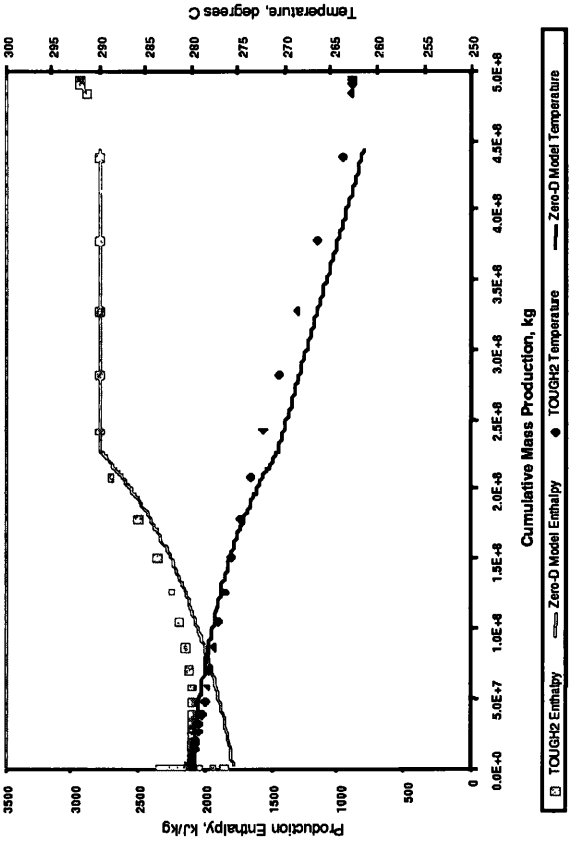

Figure 7. Production enthalpy and production temperature profiles: $s_{wi} = 0.4$; $s_{wr} = 0.2$.

temperature profiles: s_{wi} = 0.5; s_{wr} = 0.2.

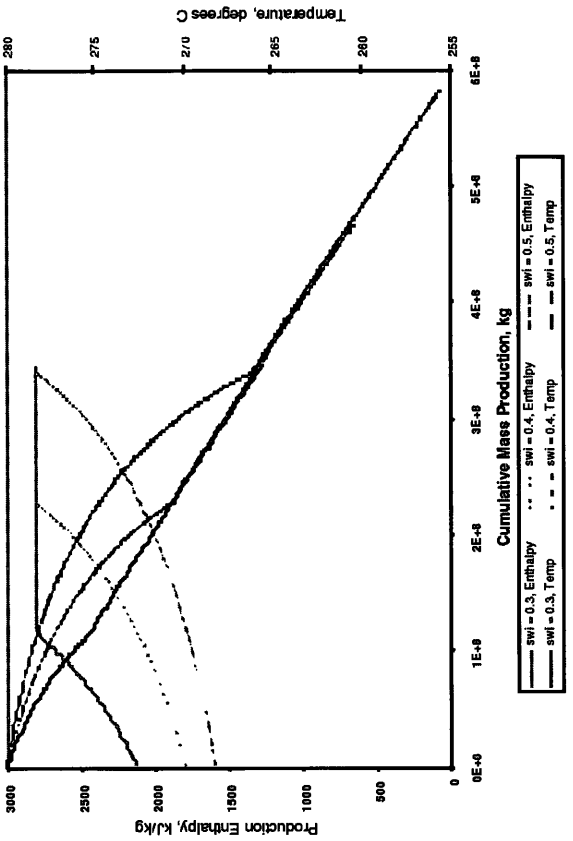

Figure 10. Zero-dimensional model production enthalpy and reservoir temperature profiles: varying s_{wi}, constant s_{wr} = 0.2.

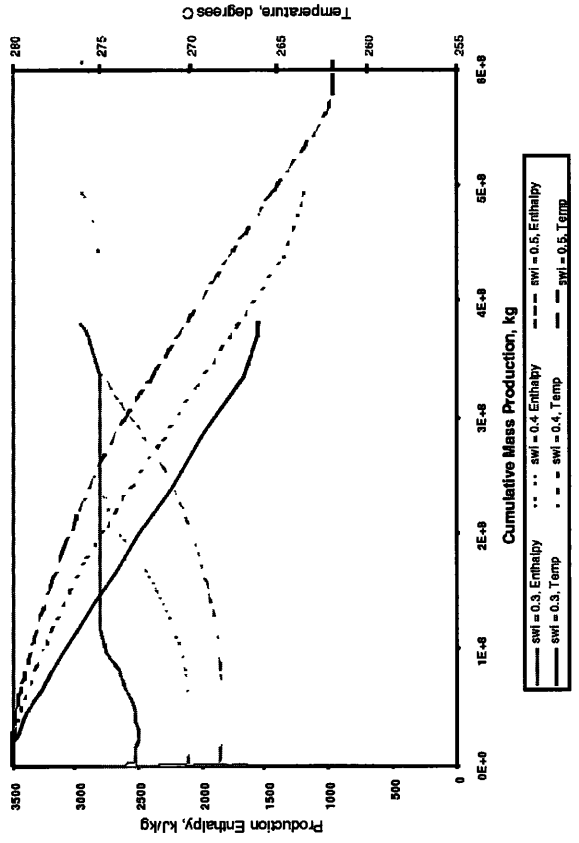

Figure 9. TOUGH2 simulated production enthalpy and reservoir temperature profiles: varying s_{wi}, constant s_{wr} = 0.2.

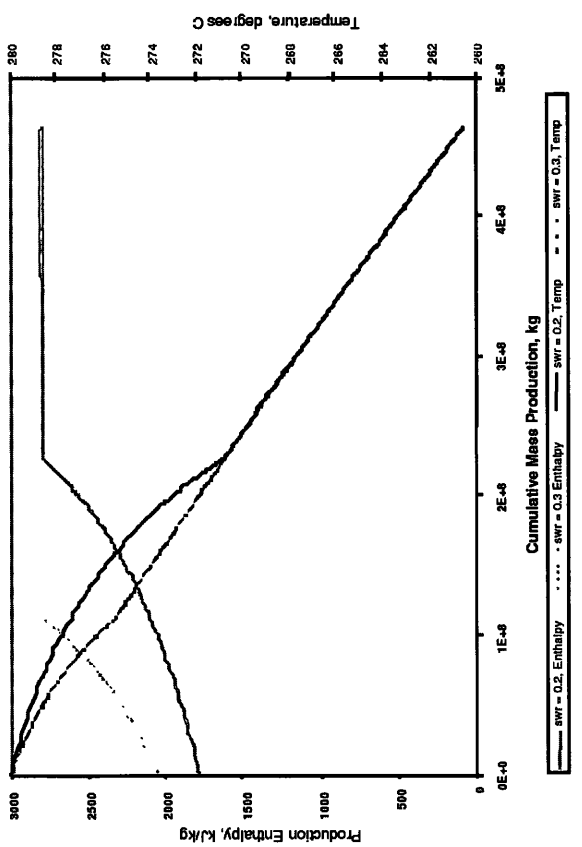

Figure 12. Zero-dimensional model production enthalpy and reservoir temperature profiles: varying s_{wr}, constant s_{wi} = 0.4.

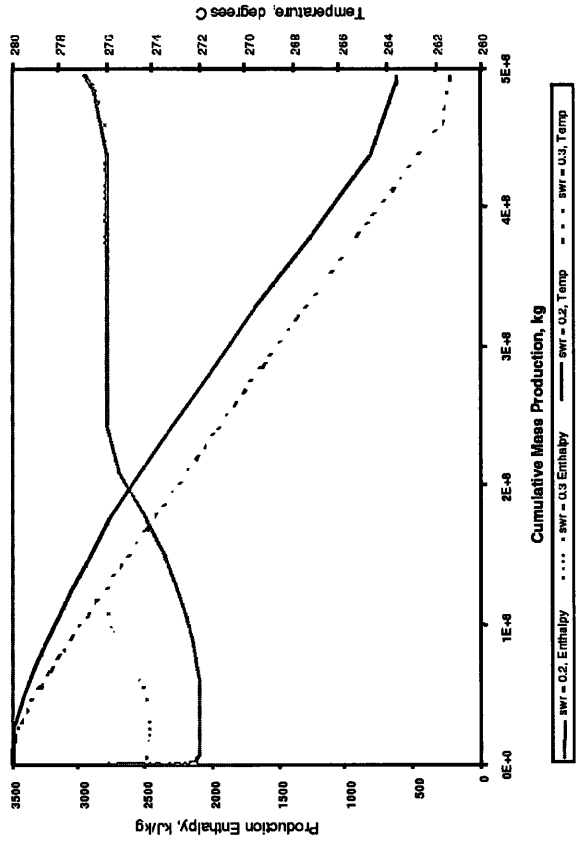

Figure 11. TOUGH2 simulated production enthalpy and reservoir temperature profiles: varying s_{wr}, constant s_{wi} = 0.4.

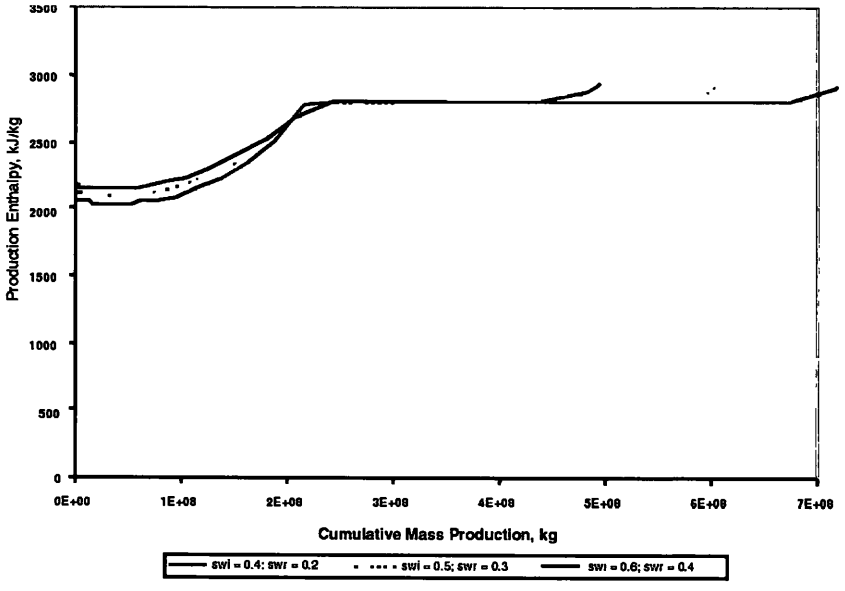

Figure 13. TOUGH2 simulated cumulative mass production and enthalpy profiles: mobile water content = 0.2.

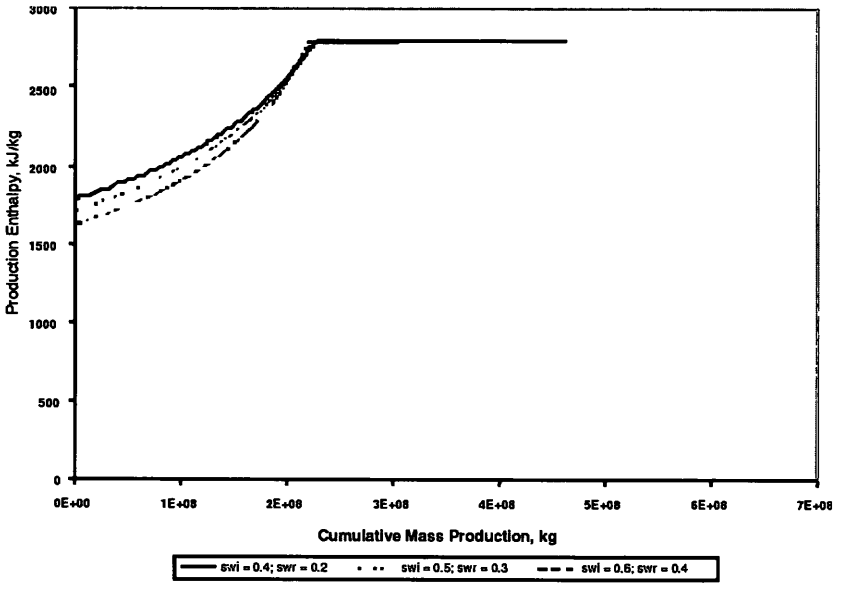

Figure 14. Zero-dimensional model cumulative mass production and enthalpy profiles: mobile water content = 0.2.